Seasonal hysteresis of surface urban heat islands

Gabriele Manoli[a,1], **Simone Fatichi**[b,c], **Elie Bou-Zeid**[d], **and Gabriel Katul**[e]

[a]Department of Civil, Environmental and Geomatic Engineering, University College London, London WC1E 6BT, UK; [b]Institute of Environmental Engineering, ETH Zurich, Zurich, Switzerland; [c]Department of Civil and Environmental Engineering, National University of Singapore, Singapore; [d]Department of Civil and Environmental Engineering, Princeton University, Princeton, NJ 08544, USA; [e]Nicholas School of the Environment, Duke University, Durham, NC 27708, USA

This manuscript was compiled on February 13, 2020

Temporal dynamics of urban warming have been extensively studied at the diurnal scale but the impact of background climate on the observed seasonality of surface urban heat islands (SUHIs) remains largely unexplored. On seasonal timescales, the intensity of urban-rural surface temperature differences (ΔT_s) exhibits distinctive hysteretic cycles whose shape and looping direction varies across climatic zones. These observations highlight possible delays underlying the dynamics of the coupled urban-biosphere system. However, a general argument explaining the observed hysteretic patterns remains elusive. A coarse-grained model of SUHI coupled with a stochastic soil water balance is developed to demonstrate that the time lags between radiation forcing, air temperature, and rainfall generate a rate-dependent hysteresis, explaining the observed seasonal variations of ΔT_s. If solar radiation is in-phase with water availability, summer conditions cause strong SUHI intensities due to high rural evaporative cooling. Conversely, cities in seasonally dry regions where evapotranspiration is out-of-phase with radiation show a summertime "oasis effect" controlled by background climate and vegetation properties. These seasonal patterns of warming and cooling have significant implications for heat mitigation strategies as urban green spaces can reduce ΔT_s during summertime, while potentially negative effects of albedo management during winter are mitigated by the seasonality of solar radiation.

Cities | Hysteresis | Seasonality | Surface Temperature | Urban Heat Island

Urban areas are generally warmer than the surrounding rural land, a phenomenon called Urban Heat Island (UHI) effect. This urban-induced warming, recognized as early as 1818 by Luke Howard (1), is one of the most evident signatures of humans' alteration of the Earth surface boundary layer. Given their implications for energy demand (2), climate adaptation policies (3), public health (4), and heat-related mortality (5, 6), UHIs have been widely studied over the past decades considering both air and surface temperature observations (e.g. 7–18). Air UHIs are most intense during nighttime, based on air temperature measurements above or below the roof level, whereas surface UHIs (hereafter referred to as SUHIs), as derived from remotely sensed skin surface temperatures, generally reach peak values during daytime (19–22). While the drivers of urban warming and its diurnal evolution are reasonably known both in terms of air and surface temperature dynamics (e.g. 8, 22–25), remote sensing observations have revealed seasonal hysteretic patterns of SUHIs that remain largely unexplained (26). The hysteresis between the intensity of SUHIs (defined as daytime urban-rural surface temperature differences, ΔT_s) and background land surface temperature (T_s) has been demonstrated by a comprehensive statistical analysis of European cities (26) and confirmed by numerical simulations for the Greater London area (27). The directionality of hysteresis is found to be clockwise (Fig. 1C), but different climatic regions exhibit distinctive hysteretic patterns with ΔT_s either increasing or decreasing with T_s depending on whether cities are located in a temperate and wet climate or a Mediterranean seasonally dry region (see Fig. 1). It is hypothesized here that this phenomenon is the result of time lags between the surface energy budget of cities, which is largely controlled by solar radiation, and the energy/water fluxes of rural areas, regulated by regional climate and vegetation seasonality (26–28). However, previous attempts to verify such hypothesis have been unsuccessful (26). This failure may be partly due to the daunting complexity of the coupled urban-biosphere system (16, 18, 29), with the emergence of hysteresis as one of its signatures (25, 30, 31).

Hysteresis has been observed in a variety of environmental processes. These include plant physiological responses to meteorological conditions (e.g. 32–35), catchment-scale dynamics of soil moisture, evapotranspiration, streamflow and solute transport (e.g. 36–39), wetting and drying of porous media (e.g. 40), soil and ecosystem carbon fluxes (e.g. 41–43), and the diurnal cycle of surface energy fluxes (e.g. 44, 45). In these contexts, the looping patterns are generally associated with time lags between a forcing and its effects on the system. Such a phenomenon is referred to as "rate-dependent" hysteresis because the system has a limited memory of the past and the hysteresis disappears in finite time if the forcing variability is suppressed. In contrast a "rate-independent" system has a persistent memory and hysteresis need not fade if the forcing term is removed. A prototypical model of rate-dependent hysteresis is given by an input-output system that transforms a sinusoidal input time series $X(t)$ into a delayed output $Y(t)$

Significance Statement

Urban heat islands represent a major threat to public health with implications for energy consumption and climate adaptation policies. A ubiquitous feature in the seasonality of surface urban heat islands (SUHIs) is distinctive hysteretic cycles between urban and rural surface temperature that still awaits a general explanation. A coarse-grained model of SUHI serving as a minimalist representation of urban-rural seasonal dynamics based on urban scaling laws and mass/energy conservation principles is proposed to explore this hysteretic behavior. It is shown that such hysteresis is controlled by time lags between energy (radiation/temperature) and water (rainfall) availability. The model largely explains the observed seasonal patterns in amplitude and looping direction and provides general guidance for SUHI reduction across cities and climates.

Author contributions: GM designed the study, conducted the analysis and wrote the manuscript with input from SF, GK, and EBZ. All authors contributed to editing the manuscript.

The authors declare no conflict of interest.

[1]To whom correspondence should be addressed. E-mail: g.manoli@ucl.ac.uk

given by

$$X(t) = \mu_X + A_X \cdot \sin\left[\omega \cdot (t + \phi_X)\right]; \quad [1]$$

$$Y(t) = \mu_Y + A_Y \cdot \sin\left[\omega \cdot (t + \phi_X + \Delta\phi)\right]; \quad [2]$$

where t is time, ω is the frequency, ϕ_X is the input phase shift and $\Delta\phi$ is the input-output time lag. In the context of the analysis here, X and Y are conceptual representations of background surface temperature and SUHI intensity, respectively. By defining normalized variables $X_n(t) = (X(t) - \mu_X)/A_X$ and $Y_n(t) = (Y(t) - \mu_Y)/A_Y$, and setting $\omega = 1$ and $\phi_X = 0$ without loss in generality, Eqs. 1-2 can be expressed as a relation between input (or forcing) $X_n(t)$ and output (or response) $Y_n(t)$ that are lagged in time by $\Delta\phi/\omega$ using (e.g. 34)

$$Y_n = X_n \cos(\Delta\phi) + \cos\left[\arcsin(X_n)\right] \sin(\Delta\phi), \quad [3]$$

where the mathematical origin of the hysteresis is the term $\arcsin(X_n)$ that can take on the same value for two distinct values of X_n except when $\Delta\phi = 0$ (leading to $Y_n = X_n$ and the loop collapses to a line). As a bridge to systems with storage (for heat, water, electric charge, etc...), Eq. 3 can be expressed as a first-order linear non-homogeneous ordinary differential equation (ODE) (e.g. 34)

$$\frac{1}{\csc(\Delta\phi)} \frac{dY_n(t)}{dt} - Y_n(t) \cos(\Delta\phi) = -X_n(t), \quad [4]$$

where storage or capacitive effects allow $dY_n(t)/dt$ to exist, and as before, a $\Delta\phi = 0$ leads to $\csc(\Delta\phi) \to \infty$, $\cos(\Delta\phi) \to 1$ and $Y_n(t) = X_n(t)$. The rate-dependency of the hysteresis is evident in this type of representation because when the "forcing" term $X_n(t)$ is removed (and the ODE becomes homogenous), $Y_n(t)$ does not exhibit loops and decays rapidly (or exponentially) in time to its zero equilibrium value. Hence, the hysteresis in Eqs. 1-2 or its equivalent form in Eq. 4 is said to be "rate-dependent". As shown in Fig. 1D-E, the conceptual model in Eqs. 1-2 produces hysteretic curves that resemble the observed seasonal patterns of ΔT_s versus T_s, thus supporting the hypothesis that a phase shift mechanism can be at the basis of SUHI seasonality. However, the factors causing these hysteretic phenomena remain to be explored and motivate the work here.

Here, this knowledge gap is bridged by combining concepts from statistical physics with urban scaling laws and basic energy conservation principles. Specifically, a stochastic soil moisture balance is coupled with a coarse-grained SUHI model to demonstrate that the manifold of observed hysteretic seasonal patterns is encoded in the time lags between energy availability (radiation/temperature) and water availability (rainfall). The urban and rural energy balances are combined to arrive at expressions linking ΔT_s to T_s for differing radiative load and precipitation. The objective is not to provide a detailed simulation of urban microclimate, which is a prerogative of urban climate models (e.g. 46) and detailed urban energy budget schemes (e.g. 47–50). Rather, the aim is to describe the temporal variability of urban-biosphere interactions in the most general terms so as to disentangle the key drivers of city-scale warming and propose general guidelines for heat mitigation strategies under different background climates (16).

Results and discussion

Seasonal dynamics. We focus the analysis on five European cities (Paris, London, Milan, Madrid, and Nicosia) that are characterized by a wide range of climatic conditions and exhibit the aforementioned hysteretic behaviors observed in Europe (26, 27). Specifically, cities in wet or relatively wet climates (Paris, London, and Milan) show a concave up hysteresis characterized by peak SUHI in summer and ΔT_s always positive, while cities in seasonally dry regions (Madrid and Nicosia) exhibit a concave down curve with peak SUHI in spring and $\Delta T_s < 0$ during summer/autumn (see Fig. 1 and results in the Supplementary Information, SI). As previously reported, annual and summer averages of ΔT_s increase with increasing mean annual rainfall (15, 17, 18) and, while Nicosia and Madrid show summer ΔT_s values that are lower than the annual mean, the opposite is observed in cities characterized by a wet climate (Fig. 2D). These trends are consistent for both daytime and mean-daily observations of SUHIs (see Fig. 2D and SI).

To test the hypothesis that hysteresis is the result of time lags between urban and rural dynamics, we have modeled background meteorological forcings (i.e. incoming shortwave radiation R_{sw}, air temperature T_a, wind speed W_s, and rainfall frequency λ_R) with sine functions $\Gamma = \Gamma(t)$ characterized by mean μ_Γ, amplitude A_Γ, and phase ϕ_Γ (see Methods). A well-established stochastic soil moisture balance (37, 51, 52) is employed to compute the seasonality of relative soil moisture (defined in standardized form by x which represents the degree of saturation in the rooting zone, see Methods), evapotranspiration (ET) and surface albedo (α) in the rural area. This probabilistic approach integrates information on rainfall daily stochasticity and seasonality to describe the "average" seasonal cycle of the different water fluxes (37). A coarse-grained SUHI model is then used to represent the changes in surface temperature caused by urbanization (18). Urban-rural surface temperature differences ΔT_s are regulated by urban-induced changes in evapotranspiration (ΔET), albedo ($\Delta\alpha$), convection efficiency (Δr_a), surface emissivity ($\Delta\varepsilon_s$), and anthropogenic heat (ΔQ_{ah}), which vary with background climate and city characteristics (see Methods and Fig. S1-S2 in the SI for details).

Despite its simplicity, the model captures the major features of the observed seasonality of water and energy fluxes at the land surface (see Fig. S3-S7 in the SI) as well as the hysteretic behavior of ΔT_s (Fig. 2B,C and Fig. S8-S9 in the SI). Model inferences suggest that magnitude and seasonality of SUHIs are largely controlled by urban-rural differences in evapotranspiration, albedo and convection efficiency (8, 15, 18). In the analyzed wet climates, the SUHI intensity is determined by ΔET (Fig. 2E and Fig. S10 in the SI) because rural ET is in-phase with radiation, it approaches potential evapotranspiration (ET_{max}) and maximizes ΔT_s during summertime by cooling the natural environment (see results in the SI). Conversely, in the analyzed seasonally dry climates, rainfall is out-of-phase with radiation causing water stress and a summertime decrease in rural ET that reduces ΔET and, as a consequence, ΔT_s (Fig. 2F and Fig. S10 in the SI). Under dry conditions, soil moisture influences not only ΔET but also modifies surface albedo by modulating the dynamics of leaf area index, LAI (see panel E in Fig. S3-S7). When LAI declines due to water stress, ΔT_s reaches its minimum due to

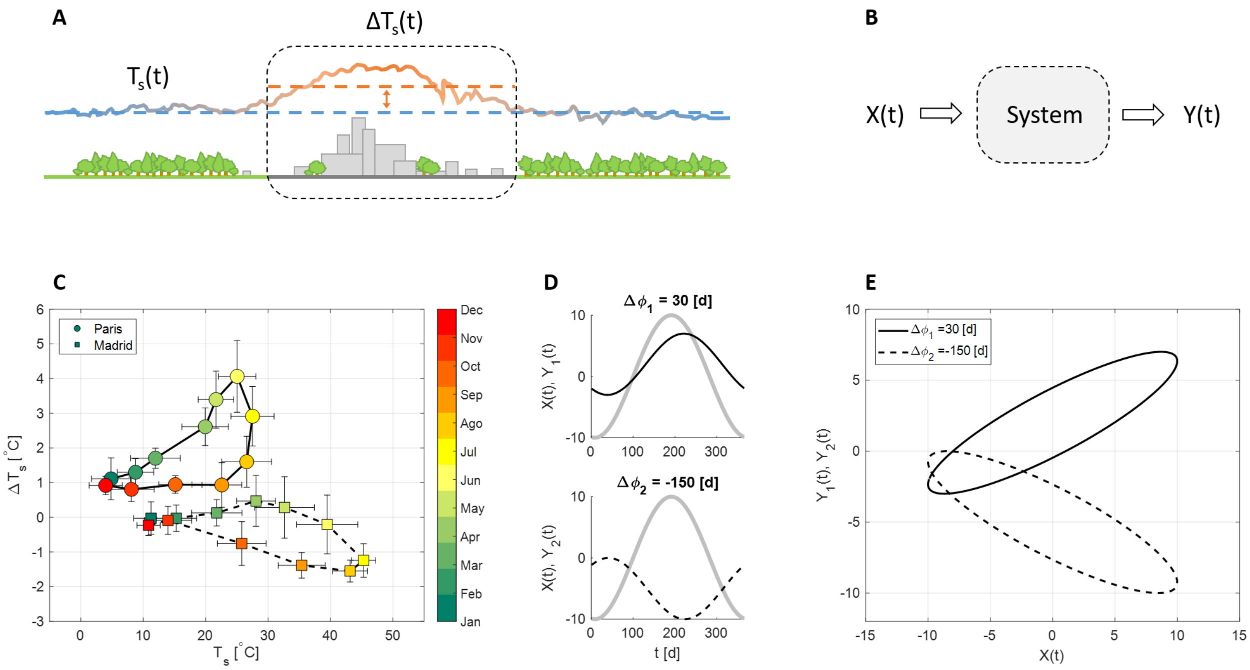

Fig. 1. (A) Conceptual representation of a daytime SUHI and (C) hysteretic behavior of ΔT_s observed in Paris (circles) and Madrid (squares). Data are digitized from Zhou et al. (26) and represent daytime values retrieved at 13:30 local time. (B) An input-output system exhibiting hysteresis: (D) time series of input X (gray line), output Y_1 (black solid line) and Y_2 (black dashed line) associated with the phase shift $\Delta\phi_1$=30 days, and $\Delta\phi_2$=-150 days, respectively; (E) resulting hysteretic curves. The input-output system is described by Eqs. 1-2 with parameters $\omega = \frac{2\pi}{365}$, μ_X=0, A_X=10, ϕ_X=-100, μ_{Y_1}=2, A_{Y_1}=5, μ_{Y_2}=-5, A_{Y_2}=5.

a delicate balance between ΔET, R_{sw}, and $\Delta\alpha$ (Fig. 2F). In such water limited ecosystems, rural vegetation is generally of low stature and changes in convection efficiency also contribute to cooling because cities can be more efficient than the surrounding "smoother" surfaces in dissipating heat by convection (15, 53). This effect, however, could be city specific as it depends on the three-dimensional structure of urban areas, the density of buildings and their mean height (e.g. 11, 54).

These results demonstrate that the shape of the hysteretic cycle is fingerprinted in the time lags between incoming shortwave radiation, temperature and rainfall. In wet climates, ET is not water limited and the hysteretic loop is mainly due to the lag between radiation and temperature ($\Delta\phi_{T_a}$), which produces a concave up curve (see Fig. S11). In seasonally dry regions, the shape of hysteresis is modified by the lag $\Delta\phi_{\lambda_R}$ between radiation and rainfall, and the induced vegetation water stress in the natural surrounding (Fig. 2-3) that generates a concave down loop. This confirms the conjecture of a phase shift mechanism (26, 55) regulated by energy and water availability. Both rainfall frequency λ_R and the lag $\Delta\phi_{\lambda_R}$ contribute to shaping the $T_s - \Delta T_s$ relation with the former controlling the magnitude of warming and the latter modifying the concavity of the hysteresis curve (Fig. 3 and Fig. S12 in the SI). Unlike previous modeling results attributing hysteresis to incoming shortwave radiation only (27), soil moisture is shown to play a key role in the seasonality of SUHIs in seasonally dry climates by linking rainfall variability to urban-rural differences in evapotranspiration and albedo. In wet regions, the impact of soil water availability is negligible due to its limited variability, and hysteresis is mainly driven by the time lag between radiation and temperature (all can be independently inferred). As a consequence, model-based results suggest that the observed hysteretic cycles are more "stable" in wet rather than dry climates as perturbations in the magnitude and seasonality of rainfall cause changes in the timing of peak maximum and minimum ΔT_s that are larger in cities like Madrid and Nicosia compared to Paris and London (see Fig. S13 in the SI). The important role of rural soil moisture in regulating urban-rural temperature differences was also detected on nocturnal UHIs, as their seasonality can be explained by changes in the thermal effusivity (or admittance (22)) of rural surfaces associated with seasonal variations in soil moisture status (56, 57).

SUHI mitigation. Given the implications of urban warming on energy consumption, climate adaptation policies, and public health, understanding and controlling UHI intensities is a leitmotif in the debate on sustainable development (59) and mitigation strategies aimed at increasing urban albedo (e.g. 15, 23, 60) or increasing urban vegetation (e.g. 61, 62) and irrigated green surfaces (63) are promoted worldwide. In this context, the coarse-grained model developed here provides a novel framework to assess the efficiency of city-scale SUHI mitigation strategies across cities, seasons, and climates. The model results suggest that increasing urban green cover ($g_{c,u}$) reduces peak warming both in wet and seasonally dry climates. When urban vegetation is irrigated, its contribution to cooling becomes dominant in seasonally dry regions where rural areas are water limited resulting in a drier regional atmosphere and lower wet-bulb temperatures in the city (Fig. 2F and Fig. 4B), while its benefits are minor in wet climates. In water scarce regions, cities are cooler not warmer than the surrounding (15, 18) and an increase in irrigated green spaces might jeopardize scarce water resources when further improvements in local micro-climate are desired. In these regions, albedo management could be a valuable alternative to counteract extreme temperatures (Fig. 4B). Future projections suggest

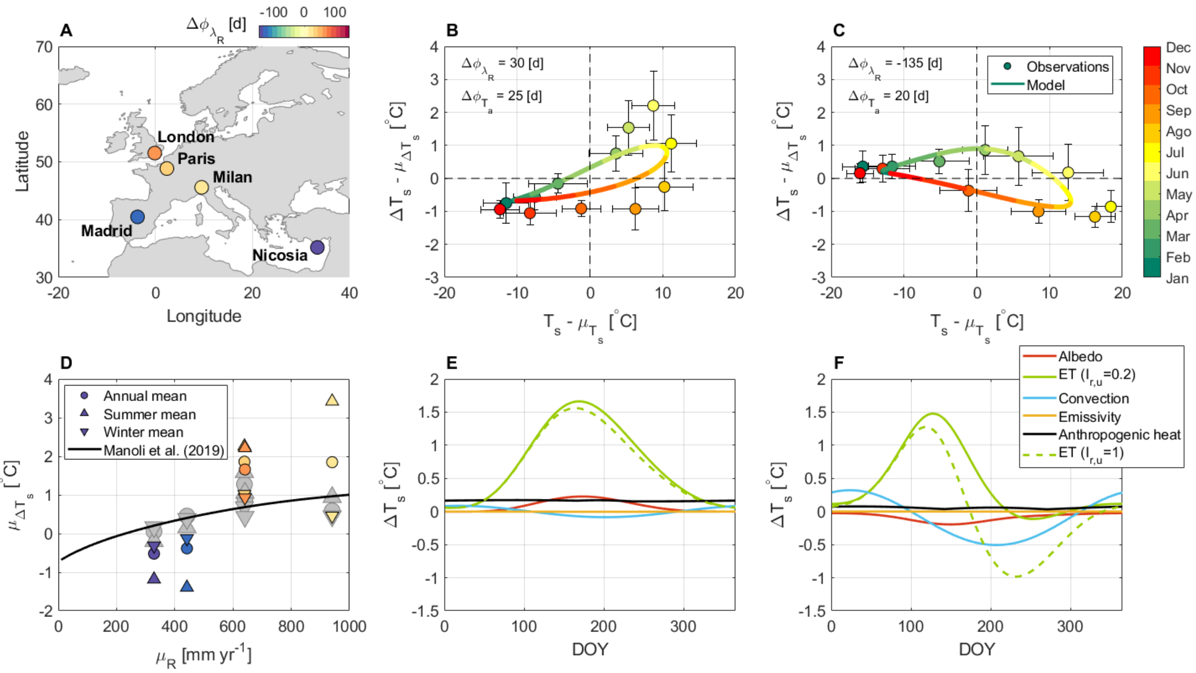

Fig. 2. (A) Location of selected European cities and observed/simulated seasonality of ΔT_s in (B) Paris (wet climate) and (C) Madrid (seasonally dry climate). Data are digitized from (26). Given that simulated quantities represent monthly averages while data are observations at 13:30 local time (26), both observations and model results in panels B-C are rescaled using their respective annual averages of surface temperature μ_{T_s} and SUHI intensity $\mu_{\Delta T_s}$ (see SI for details). Mean annual, summer, and winter intensities of SUHIs are illustrated in panel D. Colored symbols in panel D show daytime observations of SUHI intensity (26) while gray symbols illustrate mean daily values retrieved from (58). The relation between mean annual rainfall μ_R and SUHI intensity proposed by Manoli et al. (18) (summer-mean daily values for world cities) is shown for reference in panel D. Panels E and F illustrates the simulated partition of ΔT_s in its main components for Paris and Madrid, respectively. The impact of urban irrigation ($I_{r,u}$=1) on urban-rural changes in evapotranspiration is also shown (green dashed lines in panels E-F). When $I_{r,u}$=1, ET from urban vegetation is equal to potential evapotranspiration. Marker colors in panels A and D indicate the assumed time lag $\Delta\phi_{\lambda_R}$ while error bars in B and C indicate $\pm$ 1 std.

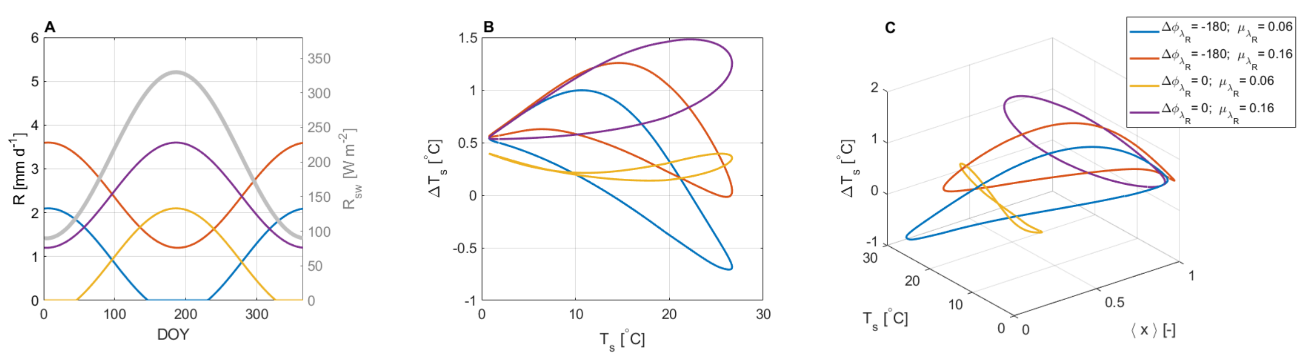

Fig. 3. Impact of different rainfall-radiation phase shifts $\Delta\phi_{\lambda_R}$ [d] and mean rainfall frequencies μ_{λ_R} [d^{-1}] on the magnitude and seasonality of urban-rural surface temperature differences ΔT_s: (A) simulated scenarios for radiation (R_{sw}) and rainfall (R), (B) simulated ΔT_s as a function of background temperature T_s, and (C) ΔT_s hysteretic cycles as a function of mean relative soil moisture $\langle x \rangle$. Simulations are performed using model parameters for the city of Madrid and the respective temperature-radiation time lag $\Delta\phi_{T_a}$ (see SI).

that world cities will grow in size and shift towards warmer and drier conditions (64, 65). Hence, the efficiency of heat mitigation strategies should be evaluated with particular care to both present and future climate scenarios as well as future trajectories of urban development and adaptation.

These results confirm that background climate-vegetation conditions influence the magnitude of SUHIs (15) and the efficiency and suitability of urban cooling strategies (18, 66). Given the seasonality of vegetation, the cooling benefits of urban green spaces are the highest during summer, i.e. when mostly needed (61), but for dry climates this optimal timing of benefits requires irrigation. Albedo modifications (i.e. highly reflective surfaces) could promote winter cooling, thus reducing the positive effects of SUHIs during cold periods when urban warming decreases energy consumption and prevents health risks associated with extreme cold (67). Nevertheless, the work here shows that negative albedo effects are dampened by the seasonality of incoming solar radiation (see Fig. 4 and Fig. S14 in the SI). This result is in line with observational and modeling evidence showing that the wintertime penalty of white roofs is negligible compared to the summer savings (68, 69) because days are shorter and the radiation load is lower.

Limitations and perspectives. While the proposed approach provides a new perspective on the seasonality of urban-induced changes in the surface energy balance, it focuses on remotely-sensed surface temperatures only and considers city-scale values, averaged in space and time over monthly timescale. Clearly, this is not sufficient to quantify thermal comfort and guide site-specific urban planning solutions. Such considerations require local air temperature, air humidity, and wind speed at the block/building scale from sub-hourly to interannual timescales (18, 50). In addition, temperature-related risks for public health largely depend on exposure and vulnerability, which vary with socio-economic conditions, travel patterns, as well as human adaptation and acclimatisation (e.g. 70, 71). Hence, the intensity of SUHI is a necessary but not sufficient metric to characterize heat stress. Mitigation efforts should also consider the overall climatic conditions experienced by citizens rather than excess urban-induced heat alone (72). Nevertheless, it is important to point out that the SUHI remains an important indicator for urban climate research as cities cannot control their background climate, but rather they can only influence the urban-induced perturbation from that background to improve their climatic conditions. The study of bulk urban properties and their interwoven relations with climate in terms of city-scale and monthly averages, as illustrated here, can provide useful insights to define guidelines and orientate interventions for cities and conditions were specific studies are not available. As the science of cities begins to mature, general results in a "mean" sense are beginning to be uncovered, which is one of the main contributions here.

Broader impact

This study demonstrates that background climate-vegetation characteristics impact not only the mean intensity of urban warming (15, 55) but also its seasonality. Many studies in the literature overlook the seasonal variability of SUHIs as the adverse impacts of urban warming are often considered to peak during summertime (13, 14). As a consequence, SUHI intensities across climatic gradients are generally reported as annual (e.g. 15) or summer/winter (e.g. 18) averages. Recently, however, it has been shown that the largest ΔT_s values occur in spring rather than summer for many cities in China (55). Similarly, many urban areas in India experience negative SUHIs during the pre-monsoon summer because of reduced rural evapotranspiration (ET) (73). Conversely, rural cooling is enhanced when the surrounding landscapes are highly irrigated (16) and during the wet season (74) when urban-rural ET differences are the highest. These results are consistent with the hysteretic patterns analyzed and explained here using a coarse-grained model. In general, the intensity of UHIs (both in terms of air and surface temperatures) is directly linked to local precipitation (15, 17, 18, 28) and "urban cool islands" generally occur in seasonally dry climates (15, 16, 73, 75) where sparse natural vegetation generates barren surfaces that have lower ET, sometimes lower albedo, and are less efficient in dissipating heat than three-dimensional urban fabrics (15, 73, 76). Urban irrigation can significantly contribute to cooling during summertime (73), but model results here suggest that urban "oasis" effects exist because of a combination of urban-rural characteristics rather than urban ET alone (75).

In conclusion, seasonal SUHIs are characterized by distinctive temporal dynamics associated with climate-vegetation conditions varying across seasons and water availability gradients. At the city scale, these mechanisms can be described by water and energy conservation principles, thus confirming that concepts and methods from ecohydrology and complex systems science can be bridged to quantify urban-induced changes in local climate (18, 77). Our results provide evidence for the hypothesis of an urban-rural phase shift mechanism (26) generated by radiation, temperature, and rainfall seasonality and causing the observed hysteretic behavior of ΔT_s. In wet regions, the phase shift between radiation and temperature largely explains the seasonality of SUHIs, while in dry climates, hysteresis is further controlled by the intra-annual variability of rainfall and its impact on soil moisture, background evapotranspiration, and albedo. For this reason, in dry climates the shape of the hysteretic curve is more susceptible to changes in the rainfall regime than in wet regions. Future modifications of background temperature and rainfall intensity/seasonality associated with global climate change may alter the current seasonality of SUHIs (78, 79) and further research is needed in this direction. Regarding SUHI mitigation, we have shown that the efficiency of different strategies vary across seasons and climate regions. Urban planning can exploit the shape of the hysteretic curve (4) as it encodes much of the processes that impact seasonal SUHI intensities. This analysis is intended to complement and not replace city-specific studies that are needed to design local-scale heat mitigation strategies and avoid negative impacts on potentially scarce water resources (63).

Materials and Methods

SUHIs and background climate. Observations of SUHIs for the cities of Paris, London, Milan, Madrid, and Nicosia are digitized from Zhou et al. (26, 55). Data represent mean monthly values of daytime SUHI intensity retrieved at 13:30 local time from 2006 to 2011. Monthly mean daily values of SUHIs calculated from daytime and nighttime observations (58) (available at https://yceo.users.earthengine.app/view/uhimap for year 2001) are also presented for comparison (Fig. 2D and results in the SI). SUHI data

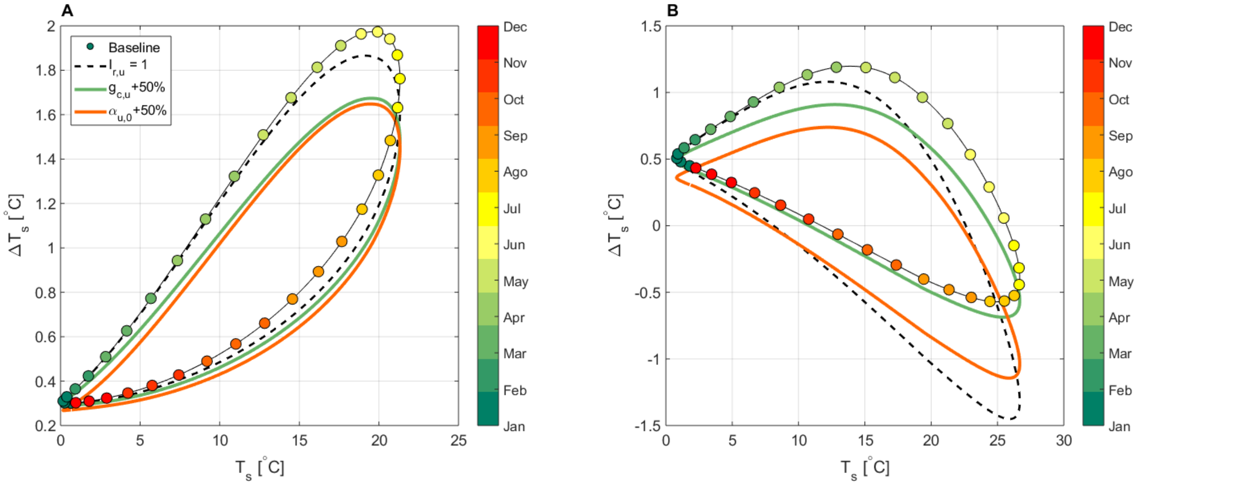

Fig. 4. Simulated seasonality of ΔT_s in (A) Paris (wet climate), and (B) Madrid (seasonally dry climate) considering different heat mitigation strategies: urban irrigation (dashed line), 50% increase in urban green cover $g_{c,u}$ (green line), and 50% increase in urban albedo $\alpha_{u,0}$ (orange line). Markers indicate the baseline scenario. In the case of irrigation ($I_{r,u}$=1), urban ET is equal to potential evapotranspiration.

are based on clear-sky conditions only so that the analysis is not representative of the full range of urban conditions experienced by cities, especially where cloudy days are frequent. Note also that seasonal variations in day length can introduce additional uncertainties in the estimated values of mean daily SUHIs as they are calculated by averaging daytime and nighttime observations (80).

To illustrate phase-shifts, we purposely represented the seasonal variability of background climate as a sine function (e.g. 81, 82), i.e. $\Gamma(t) = \mu_\Gamma + A_\Gamma sin\left[\omega \cdot (t + \phi_\Gamma)\right]$, where Γ is a stand-in variable for $R_{sw}(t)$, $T_a(t)$, $W_s(t)$, and $\lambda_R(t)$, μ_Γ is the variable mean, A_Γ is the amplitude, ϕ_Γ is the phase shift and $\omega = \frac{2\pi}{\tau}$ with period τ=365 days. The time lag between shortwave radiation and rainfall is defined as $\Delta\phi_{\lambda_R} = \phi_{R_{sw}} - \phi_{\lambda_R}$. Similarly, the time lag between radiation and temperature is $\Delta\phi_{T_a} = \phi_{R_{sw}} - \phi_{T_a}$. Sine functions for each city are fitted to monthly meteorological data retrieved from the Modern Era Retrospective-Analysis for Research and Applications (MERRA) (83). Consistent with prior studies (26), data for years 2006-2011 are used. Rainfall seasonality does not always follow clear sinusoidal trends and the selected sine functions should be considered as prototypical examples of intra-annual variability rather than matching exactly site-specific conditions. Also, the focus here is on two contrasting climatic conditions defined as “wet" and “seasonally dry" to highlight the occurrence of distinctive hysteretic patterns. The former indicates continental/temperate regions with summer rainfall and vegetation in well-watered conditions throughout the year or for a large part of it, while the latter indicates Mediterranean climates characterized by dry summers and prolonged water-limitation to evapotranspiration. However, more complex seasonal dynamics occur on continental scales (26) where bimodal rainfall patterns (84) and agriculture/irrigation in rural areas (16) may alter the hysteretic cycles illustrated here. Also, hysteresis is likely to disappear in aseasonal tropical regions where rainfall and temperature are relatively constant throughout the year. Land surface diagnostics by MERRA are then employed to assess the accuracy of simulated background albedo, leaf area index, and evapotranspiration (see SI). Mean monthly surface temperature is estimated from air temperature assuming a linear relation, i.e. $T_s(T_a) = a_T \cdot T_a + b_T$ (18).

Mathematical model. The mathematical model is structured as follows. First a stochastic soil moisture balance is solved on daily time scales to describe the seasonal dynamics of soil water, evapotranspiration, leaf area index, and surface albedo in rural areas. Then, urban-induced changes in surface temperature ΔT_s are estimated by means of a coarse-grained SUHI model that accounts for urban-rural changes in surface albedo, emissivity, evapotranspiration, convection efficiency, and anthropogenic heat. This framework provides a fully coupled description of the urban-rural system linking rainfall statistics and soil moisture dynamics to seasonal SUHI variations via changes in ET and albedo. Further details on the model development are now presented.

Stochastic soil water balance. At daily timescales, the degree of saturation (s) dynamics can be described by a dominant balance between intermittent rainfall pulses (R), evapotranspiration (ET), leakage and runoff (LQ) (51, 52), i.e.

$$nZ_r\frac{ds(t)}{dt} = R(t) - ET(s(t),t) - LQ(s(t),t); \qquad [5]$$

where n is soil porosity and Z_r the rooting depth. On daily time scales, rainfall R [mm d^{-1}] can be modeled as a marked Poisson process with frequency λ_R [d^{-1}] and events characterized by a random rainfall depth with exponential distribution of mean a [mm]. Given the stochastic nature of rainfall, Eq. 5 requires a solution in probabilistic terms (37, 51, 52). Defining a standardized relative soil moisture $x(t) = (s(t) - s_w)/(s_1 - s_w)$, where s_w is the wilting point and s_1 is a threshold around field capacity, considering temporal averages $\langle x(t)\rangle$ taken from an ensemble of stochastic rainfall realizations, and neglecting daily fluctuations around the mean, Eq. 5 can be rewritten as:

$$\frac{d\langle x(t)\rangle}{dt} = \frac{\lambda_R(t)}{\gamma(t)} - k(t)\langle x(t)\rangle - \frac{\lambda_R(t)}{\gamma(t)}e^{-\gamma(t)(1-\langle x(t)\rangle)}; \qquad [6]$$

where $\gamma(t) = \frac{w_0}{a(t)}$ is the soil storage index, $k(t) = \frac{ET_{max}(t)}{w_0}$ is the normalized potential evapotranpiration, and $w_0 = nZ_r(s_1 - s_w)$ is the maximum plant-available soil water storage. Potential evapotranspiration ET_{max} is computed from monthly mean shortwave radiation R_{sw} [MJ m^{-2} d^{-1}] and air temperature T_a [°C] with the Turc model (85, 86), i.e. $ET_{max}(t) = 0.013 \cdot \frac{T_a(t)}{T_a(t)+15}\left(23.89 \cdot R_{sw}(t) + 50\right)$ [mm d^{-1}].

Eq. 6 is a nonlinear ODE that can be solved numerically starting from an initial condition $\langle x(t_0)\rangle$ once the model parameters are known. To ensure a consistent value of the initial condition, a spin-up simulation of 5 years is run, thus eliminating any influence of $\langle x(t_0)\rangle$ on the simulated seasonal patterns. To keep the model simple, a constant rainfall depth per event $a(t)$=15 mm is employed and only the number of events is assumed to vary among cities (i.e., λ_R). The value of a is consistent with the assumption of γ=5.5 employed in the literature (37, 51).

Coarse-grained SUHI model. The intensity of SUHIs can be derived from the surface energy balance considering urbanization as a a first-order perturbation to the rural base state. Specifically, following the derivation by Manoli et al. (18), urban-rural surface temperature differences ΔT_s can be expressed as:

$$\Delta T_s(t) = \frac{1}{f_s(t) - \frac{\gamma}{a_T}f_a(t)}\Delta S(t); \qquad [7]$$

where f_s and f_a [W m^{-2} K^{-1}] are energy redistribution factors associated with surface and air temperature, respectively (87), ΔS [W m^{-2}] is the differential energy forcing due to urban-induced changes in the surface energy balance and γ and a_T are parameters accounting for the coupling between T_s and T_a. The ΔT_s in Eq. 7 represent mean daily values of SUHI intensity as daytime/nighttime conditions are smoothed over on monthly timescales and heat storage effects are neglected (18).

To directly link evapotranspiration to incoming solar radiation, the model presented by Manoli et al. (18) is modified by neglecting changes in ET due to ΔT_s (87), i.e. $ET(T_s + \Delta T_s) = ET(T_s) + \frac{dET}{dT_s}\Delta T_s + ... \simeq ET(T_s)$. Under this assumption, the terms in Eq. 7 become:

$$\Delta S(t) = -R_{sw}(t)\Delta\alpha(t) + \sigma(\varepsilon_a T_a(t)^4 - T_s(t)^4)\Delta\varepsilon_s - \lambda\Delta ET(t) + \\ + \rho c_p \frac{T_s(t) - T_a(t)}{r_a(t)^2}\Delta r_a(t) + \Delta Q_{ah}(t) \quad [8]$$

and

$$f_s(t) = \frac{\rho c_p}{r_a(t)} + 4\sigma\varepsilon_s T_s(t)^3; \quad [9]$$

$$f_a(t) = \frac{\rho c_p}{r_a(t)} + 4\sigma\varepsilon_s\varepsilon_a T_a(t)^3; \quad [10]$$

where Δ is a perturbation reflecting urban-rural differences, σ is the Stefan-Boltzmann constant, ε_s and ε_a are the land surface and atmosphere emissivities, respectively, ρ is the mean air density, r_a is the aerodynamic resistance, c_p is the specific heat of air at constant pressure, and $\Delta Q_{ah} \sim Q_{ah,u}$, with $Q_{ah,u}$ the anthropogenic heat flux from the urban surface.

A description of the different terms in Eq. 8 is provided below while model parameters are listed in the SI (Table S1). Results presented in the SI demonstrate that the assumption of a negligible $ET - \Delta T_s$ feedback is reasonable at the city and monthly scale and the modified model version is capable of reproducing the global ΔT_s patterns reported elsewhere (18).

Changes in albedo are computed as $\Delta\alpha(t) = \alpha_u(t) - \alpha(t)$, where α_u is the mean urban albedo. To account for the impact of vegetation on (snow-free) rural albedo, Rechid et al. (88) proposed the following relation:

$$\alpha(t) = \alpha_{soil}e^{-0.5\cdot LAI(t)} + \alpha_{canopy}\cdot\left(1 - e^{-0.5\cdot LAI(t)}\right); \quad [11]$$

where LAI is the leaf area index assumed to vary linearly with ET, i.e. $LAI(t) = a_1 + a_2 \cdot ET(t)$, where a_1 and a_2 are model parameters. Although simplistic, this approach provides reasonable estimates of albedo seasonal dynamics (see Fig. S3-S7 in the SI) and is considered adequate for the purpose of this study. The urban albedo is computed as:

$$\alpha_u(t) = (1 - g_{c,u})\cdot\alpha_{u,0} + g_{c,u}\cdot\alpha_{gc}(t); \quad [12]$$

where $g_{c,u}$ is the urban green cover and $\alpha_{u,0}$ is the average albedo of the urban surface. The albedo of the urban green cover, α_{gc}, is computed using Eq. 11 but considering the LAI and ET of urban vegetation.

Rural evapotranspiration is calculated as $ET(t) = \langle x(t)\rangle ET_{max}(t)$ and urban-rural changes in ET are computed as $\Delta ET(t) = g_{c,u}ET_u(t) - g_c ET(t)$ where $g_c \sim 1$ is the rural green cover and evapotranspiration by urban vegetation is defined as:

$$ET_u(t) = ET(t) + I_{r,u}\cdot(ET_{max}(t) - ET(t)); \quad [13]$$

with $I_{r,u}$ an irrigation index varying between 0 (natural conditions) and 1 (no water supply limitations so that $ET_u = ET_{max}$).

Urban emissivity ($\varepsilon_{s,u}$) and aerodynamic resistance ($r_{a,u}$) are calculated according to Manoli et al. (18). The mean building height ($h_{c,u}$) of each city is computed considering the scaling of $h_{c,u}$ with population N (89) and then employed to estimate the aerodynamic resistance, $r_{a,u}$, the sky view factor v_{sky}, and $\varepsilon_{s,u}$. To account for the effect of building density on surface roughness, the parameterization proposed by Macdonald et al. (90) is used in the calculation of $r_{a,u}$. The rural aerodynamic resistance is computed considering an average vegetation height h_c that varies depending on climate and well established height-based parameterizations for roughness (18).

The anthropogenic heat flux generated by urban areas is known to increase with population density $\rho_N = N/A_u$ (e.g. 91–94), i.e. $Q_{ah,u} \sim q_{ah,u}(T_{a,u})\cdot\rho_N$, where A_u is the urban area, $T_{a,u}$ the urban air temperature, and $q_{ah,u}$ accounts for metabolic, vehicle, and building heat emission rates. Assuming that $T_{a,u} \sim T_a$, seasonal variations in heat emissions (e.g. associated with variations in the energy demand of buildings) are modeled as $q_{ah,u}(T_a) = a_{q0} + a_{q1}CDD(T_a) + a_{q2}HDD(T_a)$ (94, 95) where $CDD = H[T_a - T^*]\cdot(T_a - T^*)$ and $HDD = H[T^* - T_a]\cdot(T^* - T_a)$ are the cooling and heating degree days, respectively, T^* is the base temperature, $H[\cdot]$ is the Heaviside step function, and a_{q0}, a_{q1}, and a_{q2} are model parameters (94). Note that the calculation of $q_{ah,u}$ on daily timescales might underestimate the actual anthropogenic flux. However, the focus here is on city-scale averages that includes low density residential zones and model results are consistent with literature values for suburban areas (see SI).

Code availability. The MATLAB code (https://www.mathworks.com/products/matlab.html) of the coarse-grained SUHI model is available on Code Ocean (https://doi.org/10.24433/CO.9808462.v1).

ACKNOWLEDGMENTS. GM was supported by the "The Branco Weiss Fellowship - Society in Science" administered by ETH Zurich. E.B.Z. acknowledges support by the Army Research Office under contract W911NF-15-1-0003 (program manager J. Barzyk), and the US National Science Foundation (NSF) under grant No. ICER-1664021 and SRN cooperative agreement No. 1444758. G.K. acknowledges support from NSF under grants No. NSF-AGS-1644382 and NSF-IOS-1754893.

1. Luke Howard. *The Climate of London: deduced from Meteorological observations, made at different places in the neighbourhood of the metropolis*, volume 1. W. Phillips, sold also by J. and A. Arch, 1818.
2. M Santamouris, C Cartalis, A Synnefa, and D Kolokotsa. On the impact of urban heat island and global warming on the power demand and electricity consumption of buildings—a review. *Energy and Buildings*, 98:119–124, 2015.
3. Francisco Estrada, WJ Wouter Botzen, and Richard SJ Tol. A global economic assessment of city policies to reduce climate change impacts. *Nature Climate Change*, 7(6):403, 2017.
4. Yvonne Rydin, Ana Bleahu, Michael Davies, Julio D Dávila, Sharon Friel, Giovanni De Grandis, Nora Groce, Pedro C Hallal, Ian Hamilton, Philippa Howden-Chapman, et al. Shaping cities for health: complexity and the planning of urban environments in the 21st century. *Lancet*, 379(9831):2079, 2012.
5. Jonathan A Patz, Diarmid Campbell-Lendrum, Tracey Holloway, and Jonathan A Foley. Impact of regional climate change on human health. *Nature*, 438(7066):310, 2005.
6. Camilo Mora, Bénédicte Dousset, Iain R Caldwell, Farrah E Powell, Rollan C Geronimo, Coral R Bielecki, Chelsie WW Counsell, Bonnie S Dietrich, Emily T Johnston, Leo V Louis, et al. Global risk of deadly heat. *Nature Climate Change*, 7(7):501, 2017.
7. Tim R Oke. City size and the urban heat island. *Atmospheric Environment (1967)*, 7(8): 769–779, 1973.
8. Timothy R Oke. The energetic basis of the urban heat island. *Quarterly Journal of the Royal Meteorological Society*, 108(455):1–24, 1982.
9. Tim R Oke. The urban energy balance. *Progress in Physical geography*, 12(4):471–508, 1988.
10. Haider Taha. Urban climates and heat islands: albedo, evapotranspiration, and anthropogenic heat. *Energy and buildings*, 25(2):99–103, 1997.
11. CSB Grimmond and Timothy R Oke. Aerodynamic properties of urban areas derived from analysis of surface form. *Journal of Applied Meteorology*, 38(9):1262–1292, 1999.
12. Menglin Jin, Robert E Dickinson, and DA Zhang. The footprint of urban areas on global climate as characterized by MODIS. *Journal of climate*, 18(10):1551–1565, 2005.
13. Marc L Imhoff, Ping Zhang, Robert E Wolfe, and Lahouari Bounoua. Remote sensing of the urban heat island effect across biomes in the continental usa. *Remote sensing of environment*, 114(3):504–513, 2010.
14. Nicholas Clinton and Peng Gong. MODIS detected surface urban heat islands and sinks: Global locations and controls. *Remote Sensing of Environment*, 134:294–304, 2013.
15. Lei Zhao, Xuhui Lee, Ronald B Smith, and Keith Oleson. Strong contributions of local background climate to urban heat islands. *Nature*, 511(7508):216, 2014.
16. Rahul Kumar, Vimal Mishra, Jonathan Buzan, Rohini Kumar, Drew Shindell, and Matthew Huber. Dominant control of agriculture and irrigation on urban heat island in India. *Scientific Reports*, 7(1):14054, 2017.
17. Yaofeng Gu and Dan Li. A modeling study of the sensitivity of urban heat islands to precipitation at climate scales. *Urban Climate*, 24:982–993, 2018.
18. Gabriele Manoli, Simone Fatichi, Markus Schläpfer, Kailiang Yu, Thomas W Crowther, Naika Meili, Paolo Burlando, Gabriel G Katul, and Elie Bou-Zeid. Magnitude of urban heat islands largely explained by climate and population. *Nature*, 573(7772):55–60, 2019.
19. TR Oke. The heat island of the urban boundary layer: characteristics, causes and effects. In *Wind climate in cities*, pages 81–107. Springer, 1995.
20. A John Arnfield. Two decades of urban climate research: a review of turbulence, exchanges of energy and water, and the urban heat island. *International Journal of Climatology: a Journal of the Royal Meteorological Society*, 23(1):1–26, 2003.
21. Donald M Yow. Urban heat islands: observations, impacts, and adaptation. *Geography Compass*, 1(6):1227–1251, 2007.

22. Timothy R Oke, Gerald Mills, Andreas Christen, and James A Voogt. *Urban Climates*. Cambridge University Press, 2017.
23. Dan Li, Elie Bou-Zeid, and Michael Oppenheimer. The effectiveness of cool and green roofs as urban heat island mitigation strategies. *Environmental Research Letters*, 9(5):055002, 2014.
24. NE Theeuwes, GJ Steeneveld, RJ Ronda, BG Heusinkveld, LWA Van Hove, and AAM Holtslag. Seasonal dependence of the urban heat island on the street canyon aspect ratio. *Quarterly Journal of the Royal Meteorological Society*, 140(684):2197–2210, 2014.
25. Kai Wang, Yuguo Li, Yi Wang, and Xinyan Yang. On the asymmetry of the urban daily air temperature cycle. *Journal of Geophysical Research: Atmospheres*, 122(11):5625–5635, 2017.
26. B Zhou, D Rybski, and Jürgen P Kropp. On the statistics of urban heat island intensity. *Geophysical Research Letters*, 40(20):5486–5491, 2013.
27. Bin Zhou, Dirk Lauwaet, Hans Hooyberghs, Koen De Ridder, Jürgen P Kropp, and Diego Rybski. Assessing seasonality in the surface urban heat island of London. *Journal of Applied Meteorology and Climatology*, 55(3):493–505, 2016.
28. IR Imamura. Role of soil moisture in the determination of urban heat island intensity in different climate regimes. *WIT Transactions on Ecology and the Environment*, 1, 1970.
29. Jianguo Liu, Thomas Dietz, Stephen R Carpenter, Marina Alberti, Carl Folke, Emilio Moran, Alice N Pell, Peter Deadman, Timothy Kratz, Jane Lubchenco, et al. Complexity of coupled human and natural systems. *science*, 317(5844):1513–1516, 2007.
30. Yosef Ashkenazy, Yizhak Feliks, Hezi Gildor, and Eli Tziperman. Asymmetry of daily temperature records. *Journal of the Atmospheric Sciences*, 65(10):3327–3336, 2008.
31. KA Morris. What is hysteresis? *Applied Mechanics Reviews*, 64(5):050801, 2011.
32. PG Jarvis. The interpretation of the variations in leaf water potential and stomatal conductance found in canopies in the field. *Phil. Trans. R. Soc. Lond. B*, 273(927):593–610, 1976.
33. A Tuzet, A Perrier, and R Leuning. A coupled model of stomatal conductance, photosynthesis and transpiration. *Plant, Cell & Environment*, 26(7):1097–1116, 2003.
34. Quan Zhang, Stefano Manzoni, Gabriel Katul, Amilcare Porporato, and Dawen Yang. The hysteretic evapotranspiration—vapor pressure deficit relation. *Journal of Geophysical Research: Biogeosciences*, 119(2):125–140, 2014.
35. Ashley M Matheny, Gil Bohrer, Paul C Stoy, Ian T Baker, Andy T Black, Ankur R Desai, Michael C Dietze, Chris M Gough, Valeriy Y Ivanov, Rachhpal S Jassal, et al. Characterizing the diurnal patterns of errors in the prediction of evapotranspiration by several land-surface models: An NACP analysis. *Journal of Geophysical Research: Biogeosciences*, 119(7): 1458–1473, 2014.
36. Valeriy Y Ivanov, Simone Fatichi, G Darrel Jenerette, Javier F Espeleta, Peter A Troch, and Travis E Huxman. Hysteresis of soil moisture spatial heterogeneity and the "homogenizing" effect of vegetation. *Water Resources Research*, 46(9), 2010.
37. Xue Feng, Amilcare Porporato, and Ignacio Rodriguez-Iturbe. Stochastic soil water balance under seasonal climates. *Proc. R. Soc. A*, 471(2174):20140623, 2015.
38. Simone Fatichi, Gabriel G Katul, Valeriy Y Ivanov, Christoforos Pappas, Athanasios Paschalis, Ada Consolo, Jongho Kim, and Paolo Burlando. Abiotic and biotic controls of soil moisture spatiotemporal variability and the occurrence of hysteresis. *Water Resources Research*, 51 (5):3505–3524, 2015.
39. G Zuecco, D Penna, M Borga, and HJ van Meerveld. A versatile index to characterize hysteresis between hydrological variables at the runoff event timescale. *Hydrological Processes*, 30(9):1449–1466, 2016.
40. Yechezkel Mualem. A conceptual model of hysteresis. *Water Resources Research*, 10(3): 514–520, 1974.
41. Shuli Niu, Yiqi Luo, Shenfeng Fei, Leonardo Montagnani, GIL Bohrer, Ivan A Janssens, Bert Gielen, Serge Rambal, Eddy Moors, and Giorgio Matteucci. Seasonal hysteresis of net ecosystem exchange in response to temperature change: patterns and causes. *Global Change Biology*, 17(10):3102–3114, 2011.
42. Quan Zhang, Gabriel G Katul, Ram Oren, Edoardo Daly, Stefano Manzoni, and Dawen Yang. The hysteresis response of soil CO_2 concentration and soil respiration to soil temperature. *Journal of Geophysical Research: Biogeosciences*, 120(8):1605–1618, 2015.
43. Quan Zhang, Richard P Phillips, Stefano Manzoni, Russell L Scott, A Christopher Oishi, Adrien Finzi, Edoardo Daly, Rodrigo Vargas, and Kimberly A Novick. Changes in photosynthesis and soil moisture drive the seasonal soil respiration-temperature hysteresis relationship. *Agricultural and Forest Meteorology*, 259:184–195, 2018.
44. CSB Grimmond, HA Cleugh, and TR Oke. An objective urban heat storage model and its comparison with other schemes. *Atmospheric Environment. Part B. Urban Atmosphere*, 25 (3):311–326, 1991.
45. Ting Sun, Zhi-Hua Wang, and Guang-Heng Ni. Revisiting the hysteresis effect in surface energy budgets. *Geophysical Research Letters*, 40(9):1741–1747, 2013.
46. CSB Grimmond, M Blackett, MJ Best, J Barlow, JJ Baik, SE Belcher, SI Bohnenstengel, I Calmet, Fei Chen, A Dandou, et al. The international urban energy balance models comparison project: first results from phase 1. *Journal of applied meteorology and climatology*, 49(6): 1268–1292, 2010.
47. Valéry Masson. A physically-based scheme for the urban energy budget in atmospheric models. *Boundary-layer meteorology*, 94(3):357–397, 2000.
48. Zhi-Hua Wang, Elie Bou-Zeid, and James A Smith. A coupled energy transport and hydrological model for urban canopies evaluated using a wireless sensor network. *Quarterly Journal of the Royal Meteorological Society*, 139(675):1643–1657, 2013.
49. Kerry A Nice, Andrew M Coutts, and Nigel J Tapper. Development of the vtuf-3d v1. 0 urban micro-climate model to support assessment of urban vegetation influences on human thermal comfort. *Urban climate*, 24:1052–1076, 2018.
50. Naika Meili, Gabriele Manoli, Paolo Burlando, Elie Bou-Zeid, Winston TL Chow, Andrew M Coutts, Edoardo Daly, Kerry A Nice, Matthias Roth, Nigel J Tapper, et al. An urban ecohydrological model to quantify the effect of vegetation on urban climate and hydrology (ut&c v1. 0). *Geoscientific Model Development Discussions*, (13):335–362, 2020.
51. Amilcare Porporato, Edoardo Daly, and Ignacio Rodriguez-Iturbe. Soil water balance and ecosystem response to climate change. *The American Naturalist*, 164(5):625–632, 2004.
52. Ignacio Rodríguez-Iturbe and Amilcare Porporato. *Ecohydrology of water-controlled ecosystems: soil moisture and plant dynamics*. Cambridge University Press, 2007.
53. Lei Zhao, Michael Oppenheimer, Qing Zhu, Jane W Baldwin, Kristie L Ebi, Elie Bou-Zeid, Kaiyu Guan, and Xu Liu. Interactions between urban heat islands and heat waves. *Environmental Research Letters*, 13(3):034003, 2018.
54. Maider Llaguno-Munitxa and Elie Bou-Zeid. Shaping buildings to promote street ventilation: A large-eddy simulation study. *Urban climate*, 26:76–94, 2018.
55. Decheng Zhou, Liangxia Zhang, Dan Li, Dian Huang, and Chao Zhu. Climate–vegetation control on the diurnal and seasonal variations of surface urban heat islands in China. *Environmental Research Letters*, 11(7):074009, 2016.
56. TR Oke, GT Johnson, DG Steyn, and ID Watson. Simulation of surface urban heat islands under 'ideal'conditions at night part 2: Diagnosis of causation. *Boundary-layer meteorology*, 56(4):339–358, 1991.
57. KE Runnalls and TR Oke. Dynamics and controls of the near-surface heat island of vancouver, british columbia. *Physical Geography*, 21(4):283–304, 2000.
58. T Chakraborty and X Lee. A simplified urban-extent algorithm to characterize surface urban heat islands on a global scale and examine vegetation control on their spatiotemporal variability. *International Journal of Applied Earth Observation and Geoinformation*, 74:269–280, 2019.
59. United Nations. New urban agenda. Conference on Housing and Sustainable Urban Development (Habitat III), Quito, Ecuador, 2017.
60. Hashem Akbari, Surabi Menon, and Arthur Rosenfeld. Global cooling: increasing world-wide urban albedos to offset CO_2. *Climatic change*, 94(3-4):275–286, 2009.
61. KR Gunawardena, MJ Wells, and Tristan Kershaw. Utilising green and bluespace to mitigate urban heat island intensity. *Science of the Total Environment*, 584:1040–1055, 2017.
62. Carly D Ziter, Eric J Pedersen, Christopher J Kucharik, and Monica G Turner. Scale-dependent interactions between tree canopy cover and impervious surfaces reduce daytime urban heat during summer. *Proceedings of the National Academy of Sciences*, page 201817561, 2019.
63. Patricia Gober, Anthony Brazel, Ray Quay, Soe Myint, Susanne Grossman-Clarke, Adam Miller, and Steve Rossi. Using watered landscapes to manipulate urban heat island effects: how much water will it take to cool Phoenix? *Journal of the American Planning Association*, 76(1):109–121, 2009.
64. E Scott Krayenhoff, Mohamed Moustaoui, Ashley M Broadbent, Vishesh Gupta, and Matei Georgescu. Diurnal interaction between urban expansion, climate change and adaptation in us cities. *Nature Climate Change*, 8(12):1097–1103, 2018.
65. Jean-Francois Bastin, Emily Clark, Thomas Elliott, Simon Hart, Johan van den Hoogen, Iris Hordijk, Haozhi Ma, Sabiha Majumder, Gabriele Manoli, Julia Maschler, et al. Understanding climate change from a global analysis of city analogues. *PloS one*, 14(7):e0217592, 2019.
66. Zhaowu Yu, Shaobin Xu, Yuhan Zhang, Gertrud Jørgensen, and Henrik Vejre. Strong contributions of local background climate to the cooling effect of urban green vegetation. *Scientific Reports*, 8(1):6798, 2018.
67. Jiachuan Yang and Elie Bou-Zeid. Should cities embrace their heat islands as shields from extreme cold? *Journal of Applied Meteorology and Climatology*, 57:1309–1320, 2018.
68. Prathap Ramamurthy, Ting Sun, Keith Rule, and Elie Bou-Zeid. The joint influence of albedo and insulation on roof performance: An observational study. *Energy and Buildings*, 93:249–258, 2015.
69. Prathap Ramamurthy, Ting Sun, Keith Rule, and Elie Bou-Zeid. The joint influence of albedo and insulation on roof performance: A modeling study. *Energy and Buildings*, 102:317–327, 2015.
70. Antonio Gasparrini, Yuming Guo, Masahiro Hashizume, Eric Lavigne, Antonella Zanobetti, Joel Schwartz, Aurelio Tobias, Shilu Tong, Joacim Rocklöv, Bertil Forsberg, et al. Mortality risk attributable to high and low ambient temperature: a multicountry observational study. *The Lancet*, 386(9991):369–375, 2015.
71. David M Hondula, Robert E Davis, and Matei Georgescu. Clarifying the connections between green space, urban climate, and heat-related mortality, 2018.
72. Alberto Martilli, E Scott Krayenhoff, and Negin Nazarian. Is the urban heat island intensity relevant for heat mitigation studies? *Urban Climate*, 31:100541, 2020.
73. Hiteshri Shastri, Beas Barik, Subimal Ghosh, Chandra Venkataraman, and Pankaj Sadavarte. Flip flop of day-night and summer-winter surface urban heat island intensity in India. *Scientific reports*, 7:40178, 2017.
74. Tirthankar Chakraborty, Chandan Sarangi, and Sachchida Nand Tripathi. Understanding diurnality and inter-seasonality of a sub-tropical urban heat island. *Boundary-Layer Meteorology*, 163(2):287–309, 2017.
75. M Georgescu, M Moustaoui, A Mahalov, and Jimy Dudhia. An alternative explanation of the semiarid urban area "oasis effect". *Journal of Geophysical Research: Atmospheres*, 116 (D24), 2011.
76. Young-Kwon Lim, Ming Cai, Eugenia Kalnay, and Liming Zhou. Observational evidence of sensitivity of surface climate changes to land types and urbanization. *Geophysical Research Letters*, 32(22), 2005.
77. JM Sobstyl, T Emig, MJ Abdolhosseini Qomi, F-J Ulm, and RJ-M Pellenq. Role of city texture in urban heat islands at nighttime. *Physical review letters*, 120(10):108701, 2018.
78. Mark P McCarthy, Martin J Best, and Richard A Betts. Climate change in cities due to global warming and urban effects. *Geophysical research letters*, 37(9), 2010.
79. Keith Oleson. Contrasts between urban and rural climate in ccsm4 cmip5 climate change scenarios. *Journal of Climate*, 25(5):1390–1412, 2012.
80. Jiameng Lai, Wenfeng Zhan, Fan Huang, James Voogt, Benjamin Bechtel, Michael Allen, Shushi Peng, Falu Hong, Yongxue Liu, and Peijun Du. Identification of typical diurnal patterns for clear-sky climatology of surface urban heat islands. *Remote sensing of environment*, 217: 203–220, 2018.
81. PCD Milly. Climate, soil water storage, and the average annual water balance. *Water Resources Research*, 30(7):2143–2156, 1994.
82. Wouter R Berghuijs, Murugesu Sivapalan, Ross A Woods, and Hubert HG Savenije. Patterns of similarity of seasonal water balances: A window into streamflow variability over a range of

time scales. *Water Resources Research*, 50(7):5638–5661, 2014.
83. Ronald Gelaro, Will McCarty, Max J Suárez, Ricardo Todling, Andrea Molod, Lawrence Takacs, Cynthia A Randles, Anton Darmenov, Michael G Bosilovich, Rolf Reichle, et al. The Modern-Era Retrospective Analysis for Research and Applications, Version 2 (MERRA-2). *Journal of Climate*, 30(14):5419–5454, 2017.
84. Wouter JM Knoben, Ross A Woods, and Jim E Freer. Global bimodal precipitation seasonality: A systematic overview. *International Journal of Climatology*, 39(1):558–567, 2019.
85. L Turc. Evaluation des besoins en eau d'irrigation, évapotranspiration potentielle. *Ann. Agron.*, 12:13–49, 1961.
86. Ludovic Oudin, Frédéric Hervieu, Claude Michel, Charles Perrin, Vazken Andréassian, François Anctil, and Cécile Loumagne. Which potential evapotranspiration input for a lumped rainfall–runoff model?: Part 2 - Towards a simple and efficient potential evapotranspiration model for rainfall–runoff modelling. *Journal of hydrology*, 303(1-4):290–306, 2005.
87. Zhenzhong Zeng, Shilong Piao, Laurent ZX Li, Liming Zhou, Philippe Ciais, Tao Wang, Yue Li, Xu Lian, Eric F Wood, Pierre Friedlingstein, et al. Climate mitigation from vegetation biophysical feedbacks during the past three decades. *Nature Climate Change*, 7(6):432, 2017.
88. Diana Rechid, Thomas J Raddatz, and Daniela Jacob. Parameterization of snow-free land surface albedo as a function of vegetation phenology based on MODIS data and applied in climate modelling. *Theoretical and applied Climatology*, 95(3-4):245–255, 2009.
89. Markus Schläpfer, Joey Lee, and Luís Bettencourt. Urban skylines: building heights and shapes as measures of city size. *Preprint at https://arxiv.org/abs/1512.00946*, 2015.
90. RW Macdonald, RF Griffiths, and DJ Hall. An improved method for the estimation of surface roughness of obstacle arrays. *Atmospheric Environment*, 32(11):1857–1864, 1998.
91. L Allen, F Lindberg, and CSB Grimmond. Global to city scale urban anthropogenic heat flux: model and variability. *International Journal of Climatology*, 31(13):1990–2005, 2011.
92. David J Sailor and Lu Lu. A top–down methodology for developing diurnal and seasonal anthropogenic heating profiles for urban areas. *Atmospheric Environment*, 38(17):2737–2748, 2004.
93. David J Sailor, Matei Georgescu, Jeffrey M Milne, and Melissa A Hart. Development of a national anthropogenic heating database with an extrapolation for international cities. *Atmospheric Environment*, 118:7–18, 2015.
94. Helen C Ward, Simone Kotthaus, Leena Järvi, and C Sue B Grimmond. Surface urban energy and water balance scheme (SUEWS): development and evaluation at two UK sites. *Urban Climate*, 18:1–32, 2016.
95. David J Sailor and Chittaranjan Vasireddy. Correcting aggregate energy consumption data to account for variability in local weather. *Environmental Modelling & Software*, 21(5):733–738, 2006.